EARTH SCIENCES
RESEARCH JOURNAL
Earth Sci. Res. J. Vol. 29, No. 3 (September, 2025):297 - 312

UNIVERSIDAD NACIONAL DE COLOMBIA

GEOPHYSICS

Study on the relationship between Global Positioning System Total Electron Content Anomalies and Earthquake Events in Thailand during Solar Cycle 24

Chollada Pansong [1,2] and Prasert Kenpankho [1*]
1. Department of Engineering Education, School of Industrial Education and Technology,
King Mongkut's Institute of Technology Ladkrabang, Bangkok 10520, Thailand
2. Department of Technical Education, Faculty of Technical Education,
Rajamangala University of Technology Thanyaburi, Pathum Thani 12110, Thailand
* Corresponding authors: prasert.ke@kmitl.ac.th

ABSTRACT

This study investigates ionospheric Total Electron Content (TEC) anomalies in relation to earthquake events in Thailand from 2007 to 2020, encompassing Solar Cycle 24. TEC data were obtained from three sources: the Global Positioning System (GPS), the International GNSS Service (IGS), and the International Reference Ionosphere (IRI), and were compared to 473 earthquakes (Mw ≥ 3.0). While earthquake magnitudes below Mw 5.0 did not exhibit a clear correlation, earthquake events of Mw 5.0 or higher reflected in moderate negative correlation coefficients for GPS TEC, IGS TEC, and IRI TEC (-0.495, -0.501, and -0.303, respectively). Furthermore, a positive correlation coefficient (0.611) was found between Mw ≥ 5.0 earthquakes and geomagnetic storms with the Kp index. However, focusing specifically on geomagnetic storms and TEC variations on the day of an earthquake, no significant relationship was detected across GPS, IGS, and IRI data. Nevertheless, further research is needed to clarify the link between seismic activity and TEC fluctuations, potentially through alternative approaches or targeted case studies. This is especially important given the limited number of earthquakes above a magnitude of 5.0 in our study area, which restricts the available sample size.

Keywords: Total electron content, Earthquake events, Solar cycle 24, Ionosphere and seismic activities, Correlation coefficient

Estudio de la relación entre las anomalías del Contenido Total de Electrones del Sistema de Posicionamiento Global y los eventos de terremoto en Tailandia durante el Ciclo Solar 24

RESUMEN

Este estudio investiga las anomalías ionosféricas del Contenido Total de Electrones (TEC) en relación con los eventos de terremoto en Tailandia entre 2007 y 2020, período del Ciclo Solar 24. La información del TEC se obtuvo de tres fuentes: Sistema de Posición Global (GPS), servicio internacional de GNSS (IGS) y el modelo de Referencia Internacional de Ionosfera, y se cotejó con 473 terremotos (Mw ≥ 3.0). Mientras que las magnitudes menores a 5.0 no presentan una clara correlación, los eventos de terremoto iguales o superiores a 5.0 reflejaron coeficientes de correlación negativa moderada para los sistemas GPS TEC, IGS TEC, e IRI TEC (-0.495, -0.501, y -0.303, respectivamente). Además, un coeficiente de correlación positiva (0.611) se encontró en los terremotos de magnitud igual o superior a 5.0. Sin embargo, en el caso específico de tormentas geomagnéticas frente a variaciones del TEC en el día de un terremoto no se detectó una relación significativa en la información del GPS, IGS e IRI. Se necesita más investigación para clarificar los vínculos entre la actividad sísmica y las fluctuaciones del TEC, potencialmente a través de acercamientos alternativos o casos de estudio específicos. Esto es especialmente importante debido al número limitado de terremotos con magnitud superior a 5.0 en esta área de estudio, lo que restringe el tamaño de la muestra.

Palabras clave: Contenido Total de Electrones; terremotos; Ciclo solar 24; ionósfera y actividades sísmicas; coeficiente de correlación.

Record
Manuscript received: 24/10/2024
Accepted for publication: 11/08/2025

How to cite this item:
Pansong, C., & Kenpankho, P. (2025). Study on the relationship between Global Positioning System Total Electron Content Anomalies and Earthquake Events in Thailand during Solar Cycle 24. *Earth Sciences Research Journal, 29*(3), 297-312. https://doi.org/10.15446/esrj.v29n3.117195

ISSN 1794-6190 e-ISSN 2339-3459
https://doi.org/10.15446/esrj.v29n3.117195

1. Introduction

Earthquakes are natural events that can occur at any time and are caused by vibrations or shaking of the Earth's surface, which people are often unable to detect. The world is likely to experience earthquakes, which can result in fatalities as well as damage to all a person's property and other buildings. Although the major plate boundary does not directly cross Thailand, the earthquake in Thailand has faults originating from the boundaries of major subplates. According to a geological study, Thailand has 16 active tectonic faults. Currently, Thailand has earthquakes more frequently. Furthermore, significant earthquakes occur in the nearby areas of Thailand, such as Indonesia, Laos, Myanmar, and the Andaman Sea. The most catastrophic incident occurred on December 26, 2004, when an earthquake in the Andaman Sea measured 9.1 to 9.3 on the magnitude scale. The earthquake caused a tsunami wave that reached several provinces, destroying homes and killing people, both domestic and international, as well as residents and visitors.

Scientists have discovered that each earthquake event influences changes in the Total Electron Content (TEC) anomaly in the ionosphere (Liu et al., 2004; Pulinets, 2004; Pulinets et al., 2005; Heki, 2011; Ouzounov et al., 2011; Priyadarshi et al., 2011; Shah & Jin, 2015; Tiryakioglu et al., 2017; Ulukavak & Inyurt, 2020; Sharma et al., 2021a; Sharma et al., 2021b; Nayak et al.,2023a; Haider et al.,2023; Nayak et al., 2024). Some analysis suggests that pressure on crustal rocks stimulates positively charged particles, causing them to travel through the troposphere and into the lower ionosphere in the direction of the surface, where they encounter electrons. Electrons may either be depleted due to attraction by positive particles or increased owing to persistent flow. Promising factors for identifying earthquake precursors include the variations and abnormalities in the behavior of ionospheric TEC that are seen before major earthquakes. Supporting evidence suggests a relationship between TEC disturbances in the ionosphere and the incidence of earthquakes, as evidenced by the behavior of TEC anomalies before major seismic events (Liu et al., 2004; Pulinets, 2004; Pulinets et al., 2005; Heki, 2011; Ouzounov et al., 2011; Priyadarshi et al., 2011; Sharma et al., 2021). TEC anomalies are typically observed after a major earthquake. However, some studies, such as Heki (2011), found that TEC changes can occur before a major earthquake. There appears to be a relationship between TEC disturbances and earthquake occurrences, as indicated by the variations and anomalies in TEC behavior that occur before major earthquakes and serve as promising parameters for detecting earthquake precursors. Dual-frequency Global Positioning System (GPS) signals can be used to analyze the delay of radio waves as they propagate through the ionosphere. This enables the analysis of earthquakes and their corresponding changes in TEC. This is accomplished by using data from ground-based receivers collected by the Global Navigation Satellite System (GNSS) (Blewitt, 1990; Kenpankho et al., 2021; Cibeira Urtiaga et al., 2022; Nayak et al., 2023b). The TEC examination reveals both positive and negative anomalies, some of which appear seven days prior to the quake. Exceeding certain thresholds, these anomalies offer compelling evidence of significant departures from typical ionospheric conditions (Nayak et al., 2023a). Researchers studied this area as follows: Heki (2011) investigated the increase in TEC preceding the 2011 Tohoku-Oki earthquake. Cahyadi and Heki (2013) identified ionospheric disturbances associated with the 2007 Bengkulu and the 2005 Nias earthquakes in Sumatra, observed by the GPS regional network. Shah and Jin (2015) presented the statistical characteristics of GPS TEC disturbances before earthquakes with a magnitude (Mw) of 5.0 or greater, covering the period from 1998 to 2014. Sharma et al. (2017) studied ionospheric TEC modeling as earthquake precursors using GNSS. Nishioka et al. (2021) conducted a statistical analysis of TEC, focusing on the long-term assessment of extreme TEC changes in Japan. Sharma et al. (2021a) developed a monitoring system for ionospheric TEC fluctuations preceding earthquakes. Sharma et al. (2021b) investigated TEC anomalies as potential earthquake precursors in Northeastern India and nearby areas, drawing on GPS data collected between 2012 and 2018. On January 15, 2022, QZSS-TEC observed ionospheric evidence of multiple atmospheric wave crossings generated by the Hunga Tonga-Hunga Ha'apai eruption in Japan. These signatures were given by Heki (2022). Xu et al. (2022) analyzed potential precursory patterns on the Earth's surface and in the atmosphere and ionosphere preceding two earthquakes with a magnitude of 7.0 and upward in Mexico in 2020-2021. Ahmed et al. (2022) studied ionospheric anomalies before the 2019 Mirpur earthquake using ionosonde measurements. Sharma et al. (2022) studied TEC anomalies before the Cuba earthquake on January 28, 2020. DeSanto et al. (2023) investigated the 2020 Simeonof earthquake in Alaska, specifically examining the limited shallow slip using GNSS-acoustic techniques. Li et al. (2023) conducted research in 2022 using M6.9 Menyuan earthquake parameters estimated from high-rate multi-GNSS. Joshi et al. (2023) investigated earthquake precursors using GNSS data and IONOLAB-TEC in the Himalayan region. Nayak et al. (2023a) examined seismo-ionospheric irregularities in large earthquakes by analyzing Vertical TEC (VTEC) from the nearest epicentral GPS stations with available PRNs. Nayak et al. (2024) observed TEC fluctuations as seismic precursors from the 2024 Noto Peninsula and Nichinan Earthquakes in Japan. Khoshgoftar and Saradjian (2024) studied multiple ionospheric, atmospheric, and surface precursors from remote sensing to improve earthquake prediction accuracy and magnitude. In addition, Sharma et al. (2024) examined the reduced ionospheric density over the epicentral region of the Mw 7.2 El Mayor-Cucapah earthquake.

Many prior investigations have demonstrated that ionospheric TEC anomalies can precede seismic events by days or weeks, providing a crucial basis for this study. For example, Shah and Jin (2015) analyzed GIM-based TEC data from 1,492 global earthquakes ($Mw \geq 5.0$) between 1998 and 2014, identifying disturbances up to five days before mainshocks. Similarly, Sharma et al. (2017) examined GNSS-derived TEC anomalies as earthquake precursors, finding deviations in ionospheric VTEC a few days before both low-magnitude (Mw 4.9) and higher-magnitude (Mw 7.8) earthquakes. Kiyani et al. (2020) investigated seismo-ionospheric anomalies linked to the 2018 Mw 8.2 Fiji earthquake using GNSS TEC, revealing low-intensity anomalies within 5-10 days before and five days after the mainshock. Beyond the five days post-event (day 7 onward), they observed a more pronounced anomaly linked to an intense geomagnetic storm, illustrating the interplay between seismic activity and geomagnetic conditions. Meanwhile, GNSS TEC dispersion following the 2011 Tohoku earthquake foreshock suggested the onset altitudes of co-seismic ionospheric disturbances, as studied by Kakinami et al. (2020). Ulukavak and Inyurt (2020) identified seismo-ionospheric precursors for strong sequential earthquakes in Nepal, noting that at magnitudes 2.0-2.5, acoustic gravity waves significantly altered TEC values, and that anomalies could last up to 30 days (15 days before and 15 days after). The ionospheric TEC also tends to decrease from five days to one day before earthquakes of Mw 6.0 or higher. Sharma et al. (2021b) indicated that earthquakes of $Mw < 5.0$ could be detected 46.50% of the time, Mw 5-6 events 81.56%, and $Mw > 6$ events fully 100%. Haider et al. (2024) employed satellite-based observations and machine learning to detect potential ionospheric and atmospheric precursors for the Mw 7.8 Turkey earthquake, integrating standard deviation (STDEV) and a nonlinear autoregressive network with exogenous inputs to identify synchronized anomalies within 6-7 days before the quake, alongside geomagnetic anomalies ($Kp > 4$; $Dst < -70$ nT; $ap > 50$ nT) on the ninth-day post-event. Nayak et al. (2024) investigated ionospheric fluctuations before an Mw 7.5 earthquake on the Noto Peninsula, detecting a significant TEC drop exceeding 5 TECU roughly 22-23 days beforehand. In addition, Sharma et al. (2024) found abnormal TEC changes within 30 days preceding an Mw 7.2 Mexico earthquake, noting a pronounced anomaly about two days prior under calm geomagnetic conditions. Collectively, these findings underscore the feasibility of TEC-based monitoring for identifying potential precursors, which we aim to adapt and refine for multi-station GPS observations in Thailand's seismic context.

In this study, we employed a GPS satellite-based approach to determine TEC values for assessing earthquake events in Thailand from 2007 to 2020, building upon prior research on TEC and ionospheric disturbances. Our main objective was to explore the relationship between earthquake magnitudes and ionospheric TEC anomalies using GPS TEC, International GNSS Service (IGS) TEC, and International Reference Ionosphere (IRI) TEC. To achieve this, we collected only dual-frequency GPS signals from 15 GNSS stations located across Thailand. Then, we calculated Slant TEC (STEC) by analyzing phase differences in the GPS L1 and L2 signals, correcting receiver and satellite biases, and converting them into VTEC. Next, we adopted a difference-based approach (dTEC) with data from the three TEC sources, comparing these values against an 11-day running average to detect TEC anomalies. Finally, external factors such as geomagnetic storms (Kp) and solar radiation were evaluated to confirm whether the observed anomalies were genuinely seismo-ionospheric. Ultimately, our research aims to guide the development of earthquake prediction and Earth observation systems in Thailand and neighboring regions.

2. Data and methodology

We compared earthquake magnitudes with GPS TEC, IGS TEC, and IRI TEC to investigate the relationship between ionospheric TEC anomalies and earthquake events. GPS TEC and IGS TEC are obtained from GPS receivers. IRI TEC is derived from the IRI model. We studied TEC disturbances associated with earthquakes in Thailand, which predominantly occur in the northern, western, and southern regions along the country's fault zones. Therefore, we need to verify the GPS TEC values against the well-known IGS TEC and IRI TEC to ensure that our GPS TEC value is suitable for use in this study. The steps involved in the research process are shown in Figure 1.

2.1 Tectonics and geology of Thailand

The Southeast Asia tectonic map in Figure 2 highlights the region's principal plate boundaries and strike-slip fault networks, which are primarily governed by the northward advance of the Indian Plate and the clockwise rotation of continental blocks around the Eastern Himalayan Syntaxis. Two prominent fault systems outside Thailand are the north-south, right-lateral Sagaing Fault in Myanmar and the northwest-southeast, left-lateral Ailao Shan-Red River (AS-RR) Fault Zone, which extends across Yunnan and Vietnam. Within Thailand, comparable large-scale faults include the Mae Ping (Wang Chao) Fault Zone, which extends over 600 km, and the left-lateral Three Pagodas Fault Zone; both likely branch from the Sagaing Fault, although their exact junction remains poorly exposed. Further south, the Ranong and Khlong Marui Fault Zones trend roughly north-south and transitioned from left- to right-lateral slip during the Oligocene-Quaternary. These faults have undergone episodic activity, exhibiting significant displacements (e.g., 120-150 km along the Mae Ping) and reactivations linked to crustal block extrusion, regional extension, and offshore basin development (Palin et al., 2013). Overall, the map illustrates how the convergence of the Indian and Eurasian Plates, coupled with strike-slip tectonics and magmatism, drives ongoing tectonic adjustments in Southeast Asia, producing a complex array of active fault zones that significantly impact regional geology and seismic hazard.

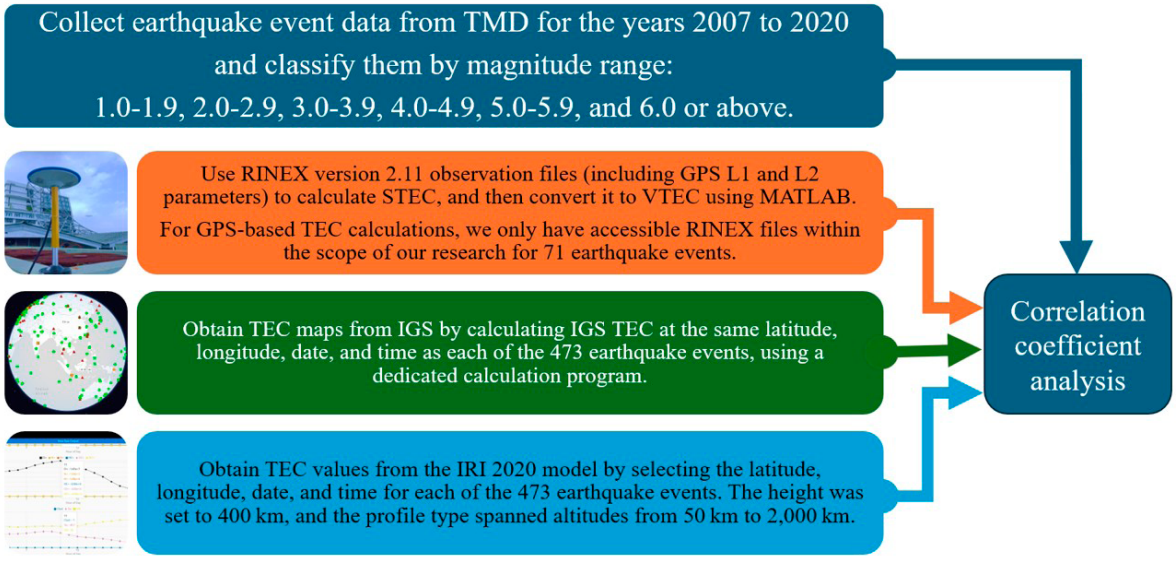

Figure 1. Workflow for earthquake data collection, classification, and TEC data analysis.

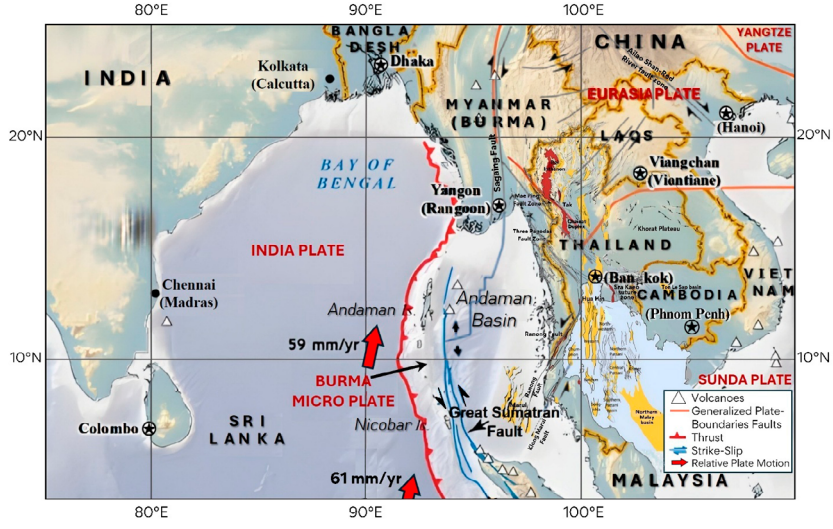

Figure 2. Presents a simplified tectonic map of Southeast Asia highlighting the major regional fault patterns, with a focus on Thailand. The map is adapted from Bernard et al. (2006), USGS (2008), Searle & Morley (2011), Palin et al. (2013), and Nachtergaele et al. (2019).

2.2 Earthquake event data

Data on earthquakes are provided by the Earthquake Observation Division (EOD) of the Thai Meteorological Department (TMD), Thailand, and can be accessed at https://earthquake.tmd.go.th/earthquakereport.html. The website provides details such as the date and time, depth, phases, latitude, longitude, magnitude, size, and region of the epicenter. Details of the earthquake occurrences in Thailand from 2007 to 2020 are shown in Table 1.

In this study, we classified earthquake magnitudes into four categories: 3.0-3.9, 4.0-4.9, 5.0-5.9, and 6.0 or greater. According to Ulukavak and Inyurt (2020), magnitudes ranging from 1.0 to 2.9 have little influence on TEC. Consequently, we focused on earthquakes of magnitude 3.0 and above, resulting in a total of 473 events recorded between 2007 and 2020 (TMD, 2023). We collected data from four regions of Thailand to examine the association between earthquake events and TEC disturbance over Thailand between the years 2007 and 2020 including 1) Southern Thailand and Andaman Sea; Southwestern Coast; Phuket, Phang Nga, Ranong, Surat Thani, Chumphon, Trang, and the Andaman Sea, 2) Western of Thailand and Andaman Sea; Western Coast; Kanchana Buri, Tak, and the Andaman Sea, 3) Northern of Thailand; Mae Hong Son, Chiang Mai, Lamphun, Chiang Rai, Payou, Lampang, Phrae, Nan, and Uttaradit, and 4) Northeast of Thailand; Nakhon Ratchasima and Loei. Table 1 shows that there were 473 earthquake events with a magnitude of 3.0 or higher in the years 2007-2020. These events were divided into 389 earthquake events with a magnitude of 3.0 to 3.9, 74 earthquake events with a magnitude of 4.0 to 4.9, eight earthquake events with a magnitude of 5.0 to 5.9, and two earthquake events with a magnitude of 6.0 and higher. The 15 GNSS stations used in this study are located along Thailand's fault lines, namely CRAI (Chiangrai: 19.57°N, 99.52°E), MAIG (Chiangmai: 19.21°N, 99.12°E), MAEH (Maehongson: 18.10°N, 97.55°E), MHSG (MaeSariang: 19.18°N, 97.58°E), NANN (Nan: 8.46°N, 100.458°E), LAMG (Lampang:18.03°N, 99.14°E), UTGN (Uttaradit:17.62°N, 100.097°E), PHEG (Phetchabun:15.46°N, 101.01°E), UTHG (Uthaithani: 15.21°N, 100.00°E), KANN (Kanchanaburi: 19.57°N, 99.52°E), BANG (Bangkok: 13.40°N, 100.36°E), PRAG (Prachuapkhirikhan: 1.56°N, 99.41°E), PHAG (Phangnga: 8.41°N, 98.15°E), PKGS (Phuket: 8.10°N, 98.31°E), and KABG (Krabi: 60°N, 98.58°E) as shown in Figure 3. Blue pins indicate them, while earthquake events with magnitudes from 2.0 to 6.0 are marked with red target pins. Yellow stars denote earthquakes, based on TMD data, and gray pins indicate magnitude 5.0 or above events from the USGS-NEIC earthquake catalogue.

The seismicity map of Thailand and adjacent regions, employed for seismic hazard assessments, integrates an earthquake catalog from USGS-NEIC, featuring subduction events (M>5) between 1922 and 2023 shown in gray, alongside TMD's earthquake catalog (2007–2023) depicted in red. Most earthquake events in Thailand occur predominantly in the northern region, which is situated along major fault lines. This area experiences a higher frequency of seismic activity compared to other parts of the country. Consequently, TMD has installed more earthquake monitoring stations in the north than in other regions. Figure 4 illustrates the focal mechanisms of earthquakes in Thailand and its surrounding regions, particularly along the major fault zones that traverse western and northern Thailand, extending to the Thai-Myanmar border. These zones are part of the larger Sagaing Fault System and its connected segments, such as Meiktila, Pyi, Nay Pyi Taw, and Bago, which all exhibit similar right-lateral strike-slip behavior. Beach-ball diagrams represent the rupture patterns and directions of subsurface rock movement, with color boundaries indicating whether a fault slips primarily in a strike-slip, reverse, or typical fashion. The region predominantly exhibits strike-slip motion, but reverse or standard components may appear depending on the stress fields associated with the collision of the Indian and Sunda Plates. Such tectonic activity exerts compressional and shear forces that keep faults in Myanmar and along the Thai-Myanmar border active; even when earthquake epicenters lie within Myanmar, their shaking can affect Thailand and potentially trigger activity in secondary faults in Thailand. Understanding these focal mechanisms is crucial for assessing fault characteristics, earthquake risk, and designing infrastructure to withstand seismic forces. Moreover, identifying whether faults are likely to slip in a strike-slip, reverse, or usual manner informs disaster preparedness measures tailored to each area's crustal deformation style. Overall, the focal mechanisms shown here highlight the dominance of right-lateral strike-slip motion. At the same time, thrust or standard components can emerge under regional stress conditions, reflecting the ongoing impact of the Indian–Sunda Plate collision on the area's geological structure.

Table 1. Earthquake events classified by magnitude and region in Thailand between 2007 and 2020.

Regions of Thailand	Magnitudes				Total
	3.0-3.9	4.0-4.9	5.0-5.9	≥ 6.0	
1. Southern Thailand and the Andaman Sea; Southwestern Coast (LAT. 7.38°N to 11.07°N, LONG. 95.15 °E to 99.66 °E)					
Phuket, Phang Nga, Ranong, Surat Thani, Chumphon, Trang, and Andaman Sea; Southwestern Coast	16	9	0	0	25
2. Western Thailand and Andaman Sea; Western Coast (LAT. 13.41°N to 17.75°N, LONG. 96.15°E to 99.34°E)					
Kanchana Buri, Tak, and Andaman Sea; Western Coast	29	7	0	0	36
3. Northern Thailand (LAT. 17.71°N to 20.40°N, LONG. 97.77°E to 101.00°E)					
Mae Hong Son, Chiang Mai, Lamphun, Chiang Rai, Payou, Lampang, Phrae, Nan, and Uttaradit	339	58	8	2	407
4. Northeast Thailand (LAT. 14.69°N to 17.62°N, LONG. 101.38°E to 101.90°E)					
Nakhon Ratchasima and Loei	5	0	0	0	5
Total	**389**	**74**	**8**	**2**	**473**

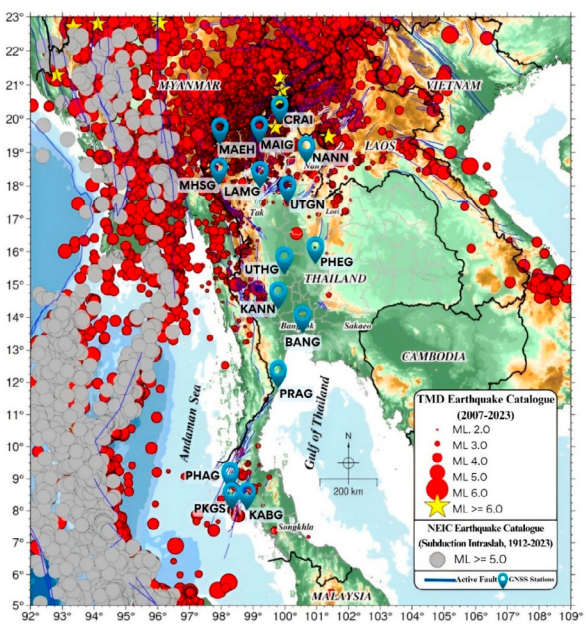

Figure 3. The illustration of earthquake magnitudes and 15 TMD GNSS stations situated along the country's fault lines, adapted from Pornsopin et al. (2024) and TMD (2023).

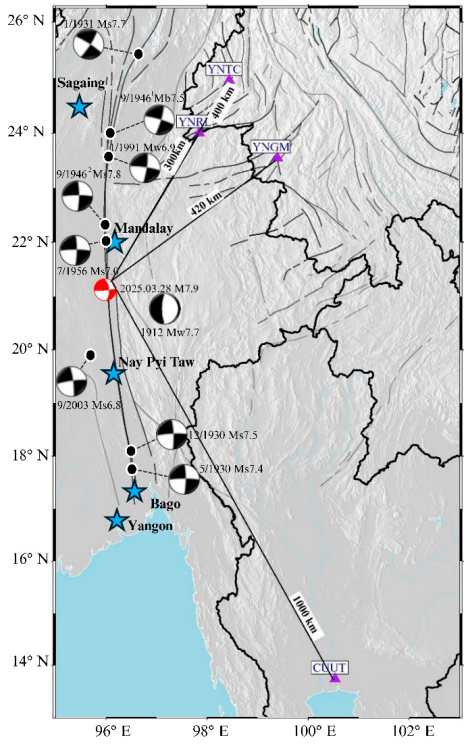

Figure 4. Focal mechanisms of earthquakes in the region of Thailand (Xiong et al., 2017; TMD, 2021; Peng et al., 2025).

2.3 GPS TEC data

GPS TEC data were selected from TMD GNSS stations that were nearest the epicenter on the day of the earthquake, with a radius of 16 km and up to 1,375 km (Pikridas et al., 2019). Regarding the relevant data, we conducted a study by collecting TEC anomalies in the ionosphere from GPS data during the earthquake's occurrence. The data was collected five days before and after the earthquake events. We have only GPS TEC data available from 2010 to 2020, corresponding to the specified days and associated with earthquakes of magnitude 3.0 and above, totaling 71 events. Although we find a correlation between TEC and earthquake events in Thailand from 2007 to 2020, the data is limited to this period. Earthquake events that matched the available GPS TEC data are shown in Table 2.

Table 2. There were 71 earthquake events with a magnitude of 3.0 and above.

TMD No.	TMD Reference ID.	Date YY-MM-DD	Time (LT)	Depth (km)	Latitude (°N)	Longitude (°E)	Locations	Magnitudes
320	TM0337	2010-04-04	23:42:52	NA	19.94	99.95	Wiang Chai, Chiang Rai	3.5
385	TM0404	2010-06-13	08:19:29	NA	14.55	99.23	Sri Sawat, Kanchanaburi	3.7
505	TM0543	2010-10-27	14:32:06	NA	14.72	99.32	Nong Prue, Kanchanaburi	3.5
568	TM0616	2011-03-24	17:49:14	NA	20.35	99.95	Chiang Rai	3.6
1009	TM1053	2011-09-28	14:40:02	NA	14.22	93.2	Andaman Sea	4.1
1010	TM1057	2011-10-01	04:22:14	NA	12.83	95.9	Andaman Sea	4.7
1011	TM1058	2011-10-01	12:48:53	NA	12.88	95.67	Andaman Sea	4.8
1012	TM1056	2011-10-01	17:54:13	NA	12.91	95.78	Andaman Sea	4.4
1014	TM1055	2011-10-03	04:34:58	NA	12.96	95.95	Andaman Sea	4.4
1189	TM1305	2012-03-30	10:39:13	NA	9.07	96.83	Andaman Sea	3.3
1218	TM1336	2012-04-16	09:44:25	NA	8.02	98.37	Thalang, Phuket	4.3
1228	TM1346	2012-04-17	05:18:45	NA	8.02	98.32	Thalang, Phuket	3.1
1231	TM1349	2012-04-17	21:15:18	NA	8.02	98.32	Thalang, Phuket	3.2
1240	TM1360	2012-04-19	19:43:41	NA	8.01	98.32	Thalang, Phuket	3.2
1243	TM1364	2012-04-20	08:10:46	NA	8.02	98.33	Thalang, Phuket	3.3
1287	TM1446	2012-06-04	05:49:04	NA	9.84	98.58	Mueang Ranong, Ranong	4.0
1670	TM1844	2013-07-05	17:49:28	NA	15.54	96.98	Andaman Sea	3.7
1739	TM1914	2013-10-10	18:19:14	NA	19.32	99.24	Phrao, Chiang Mai	4.1
1796	TM1972	2014-01-16	05:18:30	NA	9.09	98.67	Ta Khun, Surat Thani	4.0
2523	TM2701	2014-06-02	04:44:29	3	18.4	100.77	Na Noi, Nan	3.6
2294	TM2469	2014-05-12	11:05:29	8	19.8	99.72	Mae Lao, Chiang Rai	5
1910	TM2089	2014-05-05	12:06:19	5	19.7	99.62	Mae suai, Chiang Rai	5.1
1913	TM2090	2014-05-05	12:20:57	NA	19.86	99.68	Mueang, Chiang Rai	5.2
1901	TM2085	2014-05-05	11:08:42	7	19.748	99.692	Mae Lao, Chiang Rai	6.3
2061	TM2140	2014-05-06	00:58:19	2	19.7	99.53	Mae suai, Chiang Rai	5.6
2060	TM2139	2014-05-06	00:50:16	20	19.73	99.69	Mae Lao, Chiang Rai	5.9
3015	TM3223	2015-01-11	01:57:26	2	14.77	98.807	Thong Pha Phum, Kanchanaburi	3.1
3257	TM3481	2015-07-14	14:25:12	4	15.01	98.47	Sangkhla Buri, Kanchanaburi	4.8
3272	TM3497	2015-07-27	03:04:17	3	17.41	101.59	Wang Saphung, Loei	3.1
3310	TM3535	2015-08-20	12:10:24	5	15	98.42	Sangkhla Buri, Kanchanaburi	4.5
3556	TM3788	2016-02-21	01:58:45	1	19.78	99.73	Mae Lao, Chiang Rai	3.2
3566	TM3805	2016-03-02	13:53:19	4	19.63	99.72	Phan, Chiang Rai	3.0
3581	TM3821	2016-03-20	15:04:20	5	9.48	98.83	Tha Chang, Surat Thani	3.3
3808	TM4053	2016-10-14	16:00:44	7	14.69	101.38	Pak Chong, Nakhon Ratchasima	3.0
3814	TM4059	2016-10-20	03:29:38	3	15.94	98.71	Umphang, Tak	3.6
3815	TM4060	2016-10-20	03:45:53	5	16.01	98.77	Umphang, Tak	3.2
3821	TM4067	2016-10-20	12:22:02	3	16.02	98.64	Umphang, Tak	3.3
3884	TM4131	2016-11-11	12:04:25	6	16.08	98.7	Umphang, Tak	3.3
4068	TM4324	2017-01-07	20:08:57	5	16.1	98.7	Umphang, Tak	3.9
4167	TM4425	2017-02-13	07:21:18	5	17.54	98.2	Tha Song Yang, Tak	3.1
4247	TM4506	2017-04-11	10:56:33	1	8.12	97.53	Andaman Sea	3.2
4256	TM4515	2017-04-22	07:57:37	3	18.35	100.87	Na Noi, Nan	3.9
4284	TM4544	2017-05-02	10:04:42	6	19.79	99.74	Mae Lao, Chiang Rai	3.1
4310	TM4570	2017-05-24	05:58:42	3	8.05	98.48	Ko Yao, Phang Nga	3.4
4388	TM4649	2017-07-12	15:07:40	10	13.41	96.15	Andaman Sea	4.3
4614	TM4882	2017-12-07	10:26:51	1	17.25	98.38	Tha Song Yang, Tak	3.5

TMD No.	TMD Reference ID.	Date YY-MM-DD	Time (LT)	Depth (km)	Latitude (°N)	Longitude (°E)	Locations	Magnitudes
4726	TM4994	2018-01-31	15:10:31	3	15.1	98.17	Sangkhla Buri, Kanchanaburi	3.2
4793	TM5061	2018-02-23	11:13:19	6	17.75	97.86	Tha Song Yang, Tak	3.2
4826	TM5096	2018-03-20	04:24:31	18	19.732	99.678	Mae Lao, Chiang Rai	3.2
4926	TM5198	2018-06-10	15:08:11	1	17.235	101.91	Wang Saphung, Loei	3.4
4981	TM5253	2018-07-20	06:36:35	10	15.06	96.69	Andaman Sea	4.0
5165	TM5443	2018-12-30	15:39:18	2	14.9	99.14	Sri Sawat, Kanchanaburi	4.9
5167	TM5445	2018-12-30	22:02:07	10	14.9	99.15	Sri Sawat, Kanchanaburi	3.0
5182	TM5478	2019-01-10	07:09:06	5	14.9	99.15	Sri Sawat, Kanchanaburi	3.3
5246	TM5546	2019-02-16	21:41:23	10	14.34	95.87	Andaman Sea	3.9
5255	TM5554	2019-02-20	05:17:18	8	19.24	99.63	Wang Nuea, Lampang	3.3
5261	TM5561	2019-02-20	06:51:24	12	19.25	99.62	Wang Nuea, Lampang	3.0
5263	TM5563	2019-02-20	07:00:25	11	19.24	99.61	Wang Nuea, Lampang	3.1
5266	TM5566	2019-02-20	08:26:38	5	19.25	99.63	Wang Nuea, Lampang	3.3
5267	TM5567	2019-02-20	09:05:41	5	19.25	99.62	Wang Nuea, Lampang	4.9
5269	TM5569	2019-02-20	10:50:56	10	19.26	99.57	Wang Nuea, Lampang	3.0
5270	TM5570	2019-02-20	10:59:03	10	19.27	99.59	Wang Nuea, Lampang	3.7
5339	TM5639	2019-03-09	07:13:02	1	14.94	99.14	Sri Sawat, Kanchanaburi	3.1
5352	TM5652	2019-03-13	17:04:39	2	19.25	99.62	Wang Nuea, Lampang	4.2
5369	TM5669	2019-03-14	14:55:19	2	19.25	99.63	Wang Nuea, Lampang	4.0
5391	TM5691	2019-03-21	19:11:30	2	19.25	99.62	Wang Nuea, Lampang	3.1
5753	TM6062	2019-10-18	14:46:25	6	18.904	99.252	Doi Saket, Chiang Mai	4.1
5809	TM6118	2019-11-20	13:35:28	10	11.076	95.168	Andaman Sea, Phuket	3.9
5810	TM6119	2019-11-20	14:06:56	10	11.026	95.157	Andaman Sea, Phuket	4.3
6162	TM6473	2020-01-17	12:45:22	2	19.664	99.723	Phan,Chiang Rai	3.0
6446	TM6758	2020-06-25	14:37:04	5	17.6	101.68	Mueang, Loei	3.8

In Table 2, we selected 71 earthquake events ranging in magnitude from 3.0 to 6.3, for which GPS TEC data (raw data from five days before the earthquake and five days after) were available. The most significant event, measuring 6.3, occurred in Mae Lao, Chiang Rai Province, Thailand. We obtained GPS TEC parameters from 15 TMD GNSS stations, prioritizing those located near the epicenters and offering the most complete datasets, thereby ensuring the highest possible data integrity for our analysis.

We obtained GPS TEC data for five days before and five days after earthquake occurrences, totaling 11 days. GPS TEC values were obtained from the Receiver Independent Exchange (RINEX) format version 2.11. In this study, TEC was calculated using an observation file of GPS parameters, including L_1, L_2, P_1 (C_1), and P_2. The VTEC is obtained by computing the STEC. VTEC is measured in TEC units (1 TECU = 10^{16} el/m²) and is based on the total number of electrons in a one-square-meter tube along the signal channel. We used Equations (1), (2), and (3) for GPS TEC computation with MATLAB programming.

Equation (1), $STEC_L$ can be used to determine the phase difference (L_1 and L_2) between the two frequencies (f_1 and f_2) to obtain STEC from satellites to the receiver (Ma & Maruyama, 2003; Kenpankho et al., 2011).

$$STEC_L = \frac{2(f_1 f_2)^2}{k(f_1^2 - f_2^2)}(L_1\lambda_1 - L_2\lambda_2) \quad (1)$$

Where the wavelengths λ_1 (0.1904 m) and λ_2 (0.2444 m) correspond to frequencies f_1 (1575.42 MHz) and f_2 (1227.60 MHz), respectively, and k, which is related to ionosphere refraction (k = 80.62 m³/s²).

Furthermore, using Equation (2), the VTEC is calculated in units of el/m² (Ma & Maruyama, 2003; Kenpankho et al., 2011).

$$VTEC = STEC_L \times \cos\chi \quad (2)$$

where χ is the zenith angle that is defined by equation (3)

$$\chi = \arcsin\left(\frac{R_E \cos\alpha}{R_E + h}\right) \quad (3)$$

Where R_E is the Earth's radius (6,378.137 km), while h is the ionospheric layer's height (428.8 km). a is also the satellite's elevation angle at the Ionospheric Pierce Point (IPP) (Ma & Maruyama, 2003; Kenpankho et al., 2021). The angles of the satellite's elevation at 15 degrees, and the TEC-biased method from Kenpankho et al. (2021) were employed.

2.4 IGS TEC data

We referred to the IGS TEC as the TEC values from the IGS. Over 500 dual-frequency GNSS stations operating constantly throughout the world form the foundation of the IGS. The IGS organization offers ionospheric products, which can be selected from TEC map data available online via the link https://cddis.nasa.gov/archive/gnss/products/ionex/YYYY/DDD/. Following that, TEC data were extracted from the IGS corresponding to selected earthquake

events with magnitudes of 3.0 or greater. This is based on earthquake event data from the TMD covering the period from 2007 to 2020. The IGS TEC data correspond to the same date, location, and times as the selected earthquake events. By consulting the IGS network map from https://igs.org/network-resources for the period of the earthquake, we identified the corresponding latitude and longitude on the ionosphere maps. The time interval between their vertices is one hour. We collected IGS TEC data spanning 11 days, covering earthquake events from five days before to five days after, for a total of 437 events.

2.5 IRI TEC data

The International Union of Radio Science (URSI) and the Committee on Space Research (COSPAR) are the sponsors of this global initiative, known as the IRI. The IRI model version 2020, also known as the IRI TEC, is available at: https://kauai.ccmc.gsfc.nasa.gov/instantrun/iri/. The model has been launched in multiple, continually updated iterations. In the ionospheric altitude range, the IRI provides daily and monthly averages for electron density, electron temperature, ion temperature, and ion composition at a specific location, time, and date. The IRI model's intended output parameters can be chosen, such as Electron density, Ratio of Ne and F2 peak density, TEC, Electron Temperature, and Height of F2 peak. The coordinates, profile type, and range, as well as optional input and desired output parameters, can be selected as TEC output, which can be entered to obtain IRI TEC data. It is required that the location, date, and time of the seismic event match the IRI input parameters. For data analysis, we compiled a total of 11 days of IRI TEC data, consisting of five days before and five days after each earthquake event, encompassing a total of 437 events.

2.6 The geomagnetic storm activities

During the period of collecting earthquake data and monitoring TEC anomalies from 2007 to 2020, we gathered information throughout Solar Cycle 24. The solar cycle represents an approximately 11-year recurrent pattern of changes in solar activity, as manifested by variations in the observed number of sunspots. Solar Cycle 24 concluded in 2020, marking the Sun's transition into Solar Cycle 25. Notably, Solar Cycle 24 was the lowest in the last 100 years, reaching a peak of 116 sunspots, significantly below the average of 179 sunspots (National Oceanic and Atmospheric Administration (NOAA), 2023; Space Weather Prediction Center (SWPC), 2023). Geomagnetic activity is also low in Solar Cycle 24. Watari (2017) conducted a study to explore the potential connection between solar activity and local seismicity. The investigation aimed to establish a potential link between solar activity and seismic events occurring in specific localized areas. No clear correlation has been found between global seismicity and solar activity. However, in small active seismic zones, a significant connection between earthquakes and solar activity is observed ($r_{sunspot}$ = -035, r_{Dst} = 0.28). The increase in shallow earthquakes in these specific seismic zones is related to variations in space weather indices. Includes sunspot number and geomagnetic indices Kp and Dst. This suggests a plausible association between solar activity and localized seismic activity (Takla & Samwel, 2023). For this reason, we collected data on solar activity and geomagnetic storms for data analysis. The Kp geomagnetic storm index data were collected from the Pushkov Institute of Terrestrial Magnetism, Ionosphere, and Radio Wave Propagation of the Russian Academy of Sciences (IZMIRAN) at the following link: https://www.izmiran.ru/ionosphere/weather/storm/ (IZMIRAN, 2023).

2.7 Correlation coefficient

Subsequently, earthquake event data were collected and categorized based on vibration near the epicenter, with levels ranging from 0 to 6 magnitudes. Finally, we utilized the magnitudes of earthquake values and TEC data to determine the relationship between earthquake magnitudes and ionospheric disturbances in GPS TEC, IGS TEC, and IRI TEC using correlation statistics. The correlation coefficient (r) can be analyzed (Mukaka, 2012) as

$$r = \frac{\sum_{i=1}^{n}(x_i - \bar{x})(y_i - \bar{y})}{\sqrt{\left[\sum_{i=1}^{n}(x_i - \bar{x})^2\right]\left[\sum_{i=1}^{n}(y_i - \bar{y})^2\right]}} \quad (4)$$

where x_i is the earthquake magnitude value in the sample, and $\bar{x}$ is the mean average of the earthquake magnitude values. y_i is the value of the TEC in a sample, $\bar{y}$ is the mean average of the TEC values. Additionally, r is the correlation coefficient of the linear relationship between the variables x and y.

The correlation coefficient can be interpreted as follows: a value near zero means no significant association, a value near positive suggests a direct relationship, and a value near negative indicates an inverse relationship. The datasets were utilized to calculate the correlation between earthquake magnitudes and TEC anomalies across Thailand. In this research, we categorized earthquake magnitudes into ranges: 3.0-3.9, 4.0-4.9, and 5.0 and higher. We selected and used the data as available in the ranges. This allowed us to compare the daily TEC values from three data sources: GPS, IGS, and IRI. We analyzed correlation coefficients to assess the strength of the relationships. The data set covered the period from 00:00 to 24:00 UT for each day during an earthquake occurrence.

3. Results

3.1 The comparison between earthquake magnitudes and GPS TEC anomalies

This study utilized GPS TEC data encompassing 71 earthquake occurrences in Thailand between 2010 and 2020. The data was obtained from GNSS receivers with RINEX files, for which we have available data. We compared GPS TEC values during these 71 earthquake events, all of which had a magnitude of 3.0 and higher, as illustrated in Figure 5 The panels (a)-(e) depict the variation of GPS TEC during the 1-5 days before the earthquake, respectively, while panels (f)-(j) show the change in GPS TEC during the 1-5 days after the earthquake, respectively.

Figure 5, a comparison of GPS TEC anomalies before and after earthquakes of different magnitudes, it can be seen that on the fifth day before the earthquake, as shown in Figure 5 (a), the TEC was higher than on the day of the quake, the TEC gradually decreased, reaching a low on the day of the earthquake, as shown in Figure 5 (e) and (f). The TEC remained low for about two days before returning to normal. The increasing TEC was calculated to be 65.15% based on a study of 71 earthquake samples over the previous 1-5 days before the earthquake. The average increase in GPS TEC for the five- to one-day period was 5.74 TECU, 2.63 TECU, 2.80 TECU, 2.63 TECU, and 1.79 TECU, respectively. Subsequently, TEC gradually decreases, reaching its lowest point on the day of the earthquake. From panels (f)-(j), it is observed that following the earthquake event, TEC gradually increases and returns to normal within 3-5 days.

3.2 The comparison between earthquake magnitudes and IGS TEC anomalies

The IGS TEC data used in this research covers Thailand earthquake events from 2007 to 2020, which were obtained from the IGS organization. As shown in Figure 6, the results indicate 473 earthquake events with a magnitude of 3.0 or higher that were correlated with IGS TEC data, including the date and location of the earthquakes. Panels (a)-(e) show the IGS TEC changes during 1-5 days before the quake, while panels (f)-(j) show the changes in IGS TEC during 1-5 days after the earthquake, respectively.

Figure 6 compares IGS TEC anomalies in the ionosphere before and after earthquakes of various magnitudes, using 11 consecutive days of IGS TEC data that exhibit a consistent trend. Notably, on the fourth day before the earthquake (Figure 6b), TEC increased, followed by a gradual decline that reached a minimum on the day of the earthquake (Figures 6c-e). This pattern indicates that TEC generally increases in the days leading up to an earthquake,

as shown in panel (6b). Specifically, 378 out of 437 events (86.3%) exhibited a TEC increase on the fourth day before the earthquake, with an average rise of approximately 5 TECU compared to the 11-day mean IGS TEC value. Subsequently, TEC continued to decrease until the day of the earthquake, before gradually returning to normal levels, as depicted in Figures 6 (f)-(j).

3.3 The comparison between earthquake magnitudes and IRI TEC anomalies

Moreover, we compared the earthquake events and the ionospheric IRI TEC disturbance. We used the IRI TEC and 437 earthquake events from 2007 to 2020. Figure 7 (a)-(e) depicts the variation of IRI TEC during the 1-5 days before the earthquake, respectively. Panels (f)-(j) show the changes in IRI TEC from 1-5 days after the earthquake, respectively.

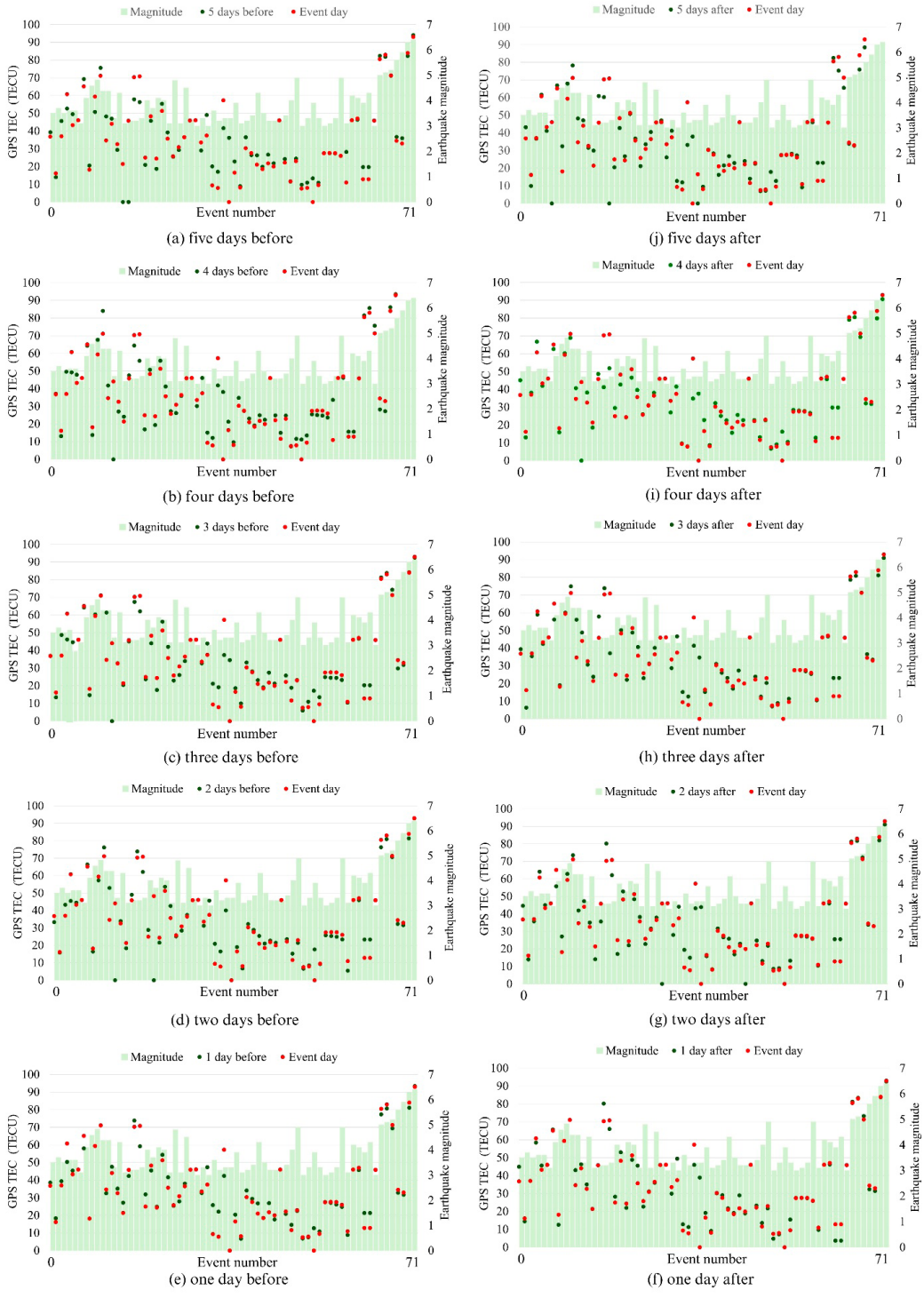

Figure 5. Comparison of GPS TEC anomalies with earthquake magnitudes, where panels (a)-(e) illustrate TEC variations during the five days preceding the earthquake, while panels (f)-(j) depict TEC changes during the five days following the earthquake events.

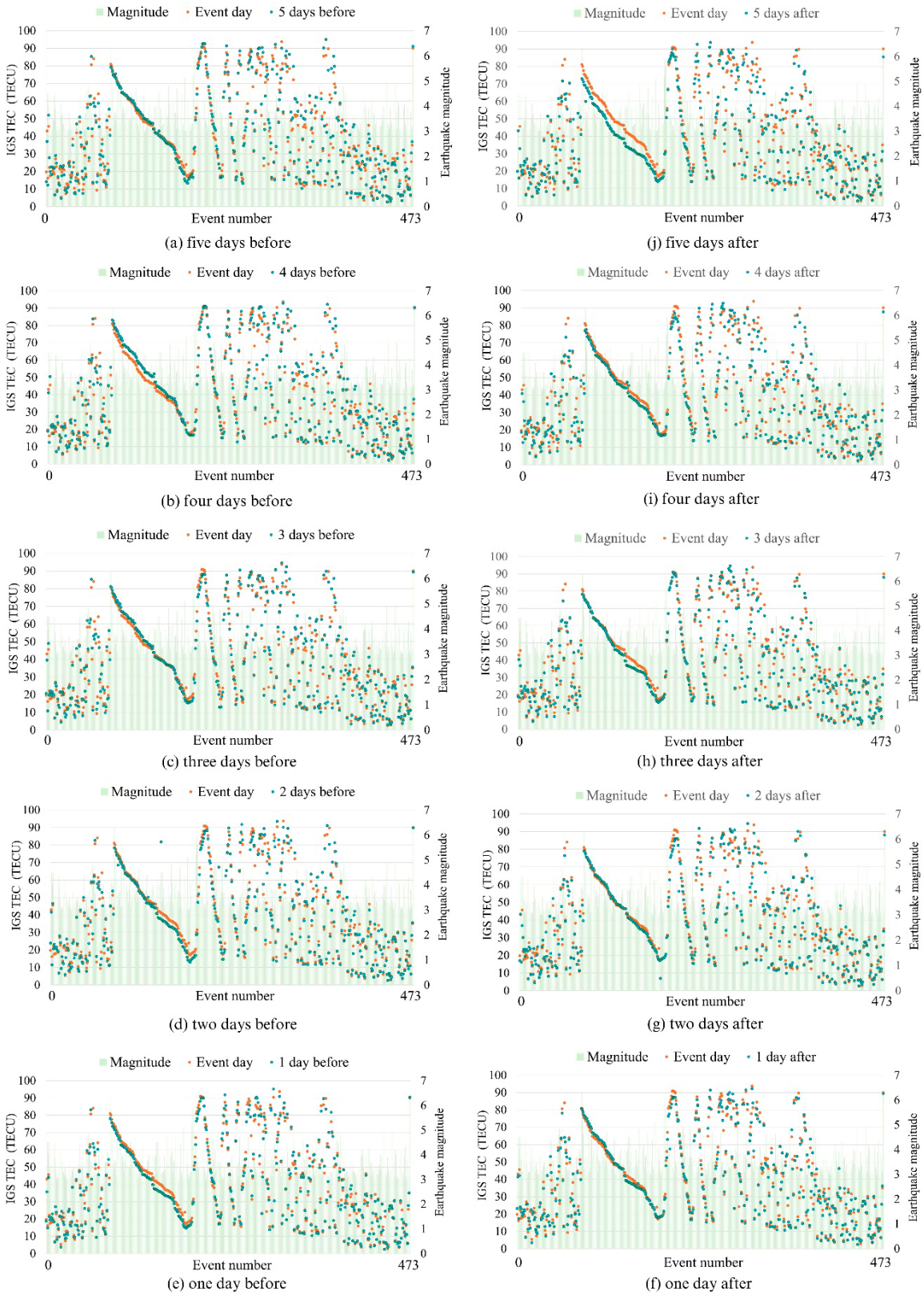

Figure 6. Comparison of IGS TEC anomalies with earthquake magnitudes, where panels (a)-(e) illustrate IGS TEC variations during the five days preceding the earthquake, while panels (f)-(j) depict IGS TEC changes during the five days following the earthquake events.

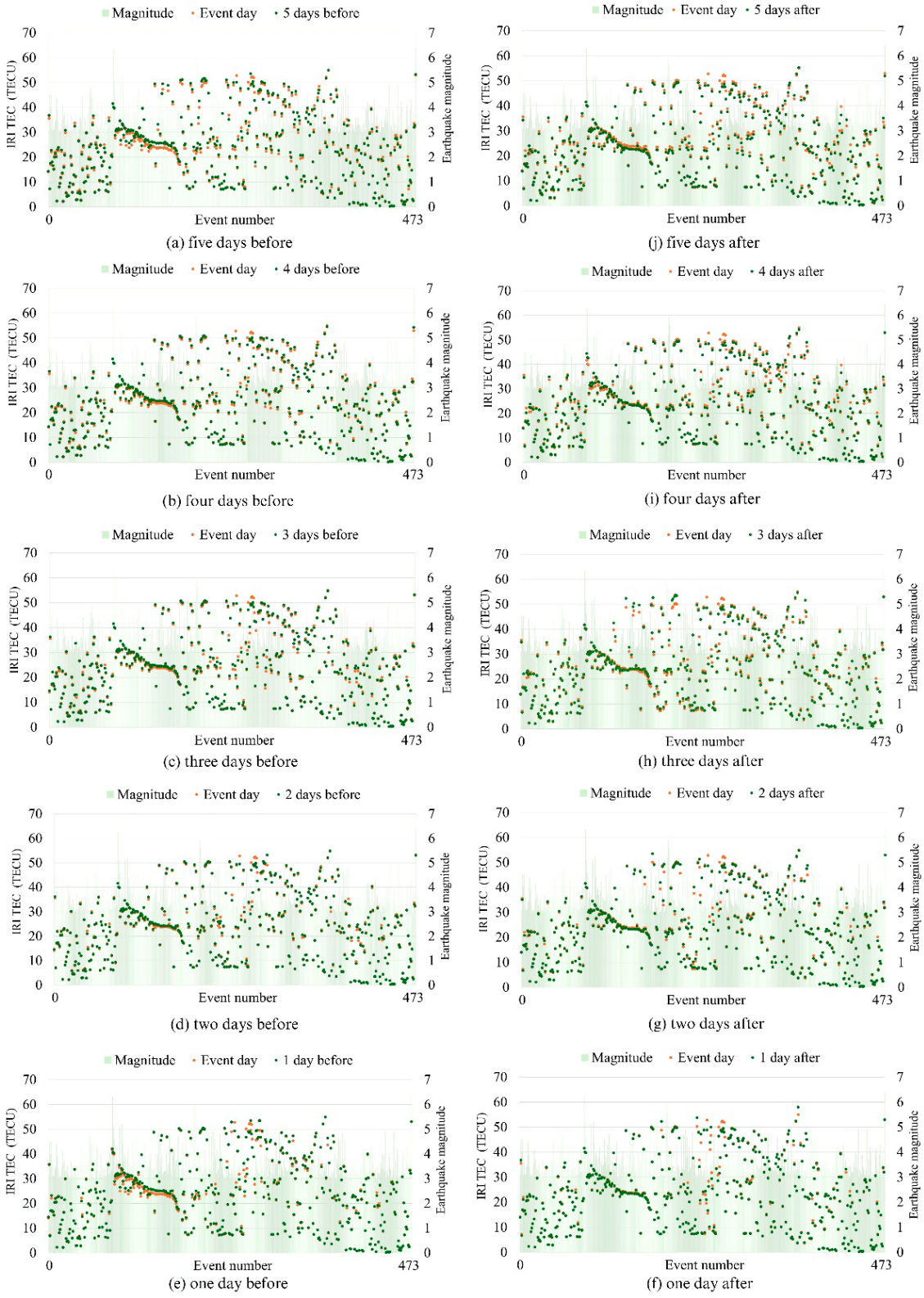

Figure 7. Comparison of IRI TEC anomalies with earthquake magnitudes, where panels (a)-(e) illustrate IRI TEC variations during the five days preceding the earthquake, while panels (f)-(j) depict IRI TEC changes during the five days following the earthquake events.

Over the 11 days, the IRI TEC values followed a consistent trend. During the five days preceding the earthquake (Figure 7a-e), TEC exhibited a slight increase, then gradually declined around the earthquake date, ultimately returning to normal levels (Figure 7f-j). Notably, in 294 out of 437 events (62.15%), TEC rose by approximately 1 TECU above the 11-day average in the five days leading up to the quake (Figure 7a). This pattern suggests that TEC generally increases before seismic events, subsequently decreases to its lowest point on the day of the earthquake (Figure 7e), and then, approximately five days afterward, begins to return to normal conditions (Figure 7j).

3.4 The relationship between earthquake magnitudes and TEC anomalies

The study examined the relationship between earthquake events and ionospheric disturbances using IGS TEC and IRI TEC data for 473 earthquake events from 2007 to 2020. However, we have access to GPS TEC data corresponding to earthquake events from 2010 to 2020, totaling 71 incidents. The relationships between earthquake magnitudes and TEC anomalies are in Table 3.

In Table 3, the correlation coefficients (r) between earthquake magnitudes and GPS TEC anomalies on the days of the earthquake (EQ) are $r_{GPS\ (EQ\ 3.0\text{-}3.9)} = -0.081$, $r_{GPS\ (EQ\ 4.0\text{-}4.9)} = -0.053$, and $r_{GPS\ (EQ\ 5.0\ and\ higher)} = -0.495$. The correlation coefficients between earthquake magnitudes and IGS TEC anomalies on the quake day are $r_{IGS\ (EQ\ 3.0\text{-}3.9)} = 0.092$, $r_{IGS\ (EQ\ 4.0\text{-}4.9)} = 0.043$, and $r_{IGS\ (EQ\ 5.0\text{-}5.9)} = -0.501$, respectively. The correlation coefficients between earthquake magnitudes and IRI TEC anomalies on the quake day are $r_{IRI\ (EQ\ 3.0\text{-}3.9)} = 0.089$, $r_{IRI\ (EQ\ 4.0\text{-}4.9)} = 0.030$, and $r_{IRI\ (EQ\ 5.0\text{-}5.9)} = -0.303$, respectively.

3.5 The comparison among earthquake magnitudes, geomagnetic storms, and TEC anomalies.

The dataset includes earthquake events of magnitude 3.0 or higher in Thailand from 2007 to 2020, encompassing the entire 24th solar cycle. In total, 437 events were identified, and geomagnetic storm data based on the Kp index were compiled to compare the frequency of geomagnetic storms with earthquake occurrences, as illustrated in Figure 8. For this study, we specifically examined space weather indices, namely sunspot number and Kp index, alongside earthquake occurrences within Thailand's geographical boundaries. The data are shown in Figure 8.

Table 3. The relationship between earthquake magnitudes and the GPS TEC, IGS TEC, and IRI TEC anomalies in the ionosphere.

Correlation coefficient / Earthquake magnitudes		5 days before	4 days before	3 days before	2 days before	1 day before	Event day	1 day after	2 days after	3 days after	4 days after	5 days after
3.0-3.9	GPS TEC	-0.123	-0.132	-0.096	-0.107	-0.103	-0.081	-0.081	-0.024	-0.117	-0.052	-0.141
4.0-4.9		-0.073	0.008	-0.087	-0.108	-0.102	-0.053	-0.080	0.024	-0.078	-0.064	0.010
5.0-higher		-0.310	-0.278	-0.274	-0.333	-0.477	-0.495	-0.314	-0.153	-0.202	-0.225	-0.220
3.0-3.9	IGS TEC	0.098	0.103	0.100	0.091	0.098	0.092	0.102	0.099	0.097	0.099	0.085
4.0-4.9		0.052	0.043	0.031	0.031	0.042	0.043	0.035	0.034	0.031	0.016	0.020
5.0-higher		-0.426	-0.562	-0.506	-0.472	-0.481	-0.501	-0.528	-0.498	-0.464	-0.514	-0.472
3.0-3.9	IRI TEC	0.095	0.093	0.092	0.092	0.093	0.089	0.089	0.086	0.087	0.091	0.085
4.0-4.9		0.023	0.027	0.022	0.030	0.014	0.030	0.023	0.025	0.024	0.018	0.021
5.0-higher		-0.266	-0.294	-0.309	-0.299	-0.299	-0.303	-0.306	-0.310	-0.277	-0.328	-0.316

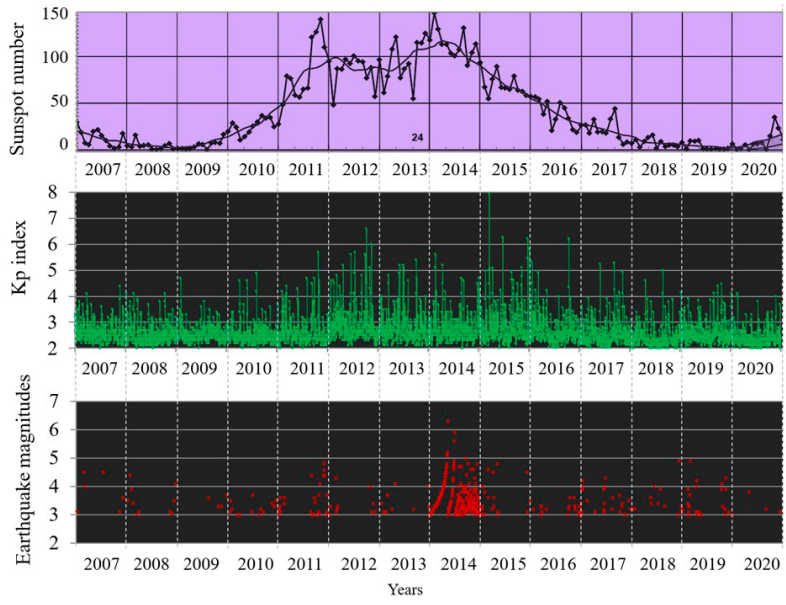

Figure 8. A total of 473 earthquakes occurred in Thailand, in comparison to geomagnetic activity, during the years 2007-2020, encompassing the period of Solar Cycle 24.

Figure 8 shows a comparison of the number of sunspots, geomagnetic storms as indicated by the Kp index, and earthquake occurrence in Thailand from 2007 to 2020. The solar cycle reached its maximum sunspot activity in 2014. The peak monthly sunspot number during this cycle occurred in April 2014, with an approximate value of 82. For the Kp index data, considering daily averages from 2007 to 2020, the number of days with geomagnetic storms rated at Kp greater than 4.0 was 127. In 2012, there were the highest occurrences of geomagnetic storms, totaling 23 days. The most intense geomagnetic storm, with a magnitude of 7.93, occurred in 2015. In the year 2014, which marked the peak of Solar Cycle 24, there was a notable increase in earthquake activity in the Thailand region. It can be observed that in 2014, a period of high solar activity coincided with the occurrence of earthquakes with magnitudes greater than 3.0 within this region, resulting in a total of 284 events. Among these earthquakes, one recorded a magnitude of 6.3 in 2014, representing the highest magnitude recorded from 2007 to 2020.

We analyzed the relationship between earthquake magnitudes and geomagnetic storm data using the Kp index. Specifically, we compared each earthquake's magnitude with the daily average Kp index on the day of the event, which categorized the dataset according to earthquake magnitudes. To analyze the correlation between geomagnetic storms (represented by the Kp index) and TEC variations on earthquake days, we examined GPS TEC, IGS TEC, and IRI TEC. Then, we grouped the TEC data by earthquake magnitude and compared these values to the corresponding Kp index on each event day. The details are presented in Table 4.

Table 4. The relationship among earthquake magnitudes, geomagnetic storms, and TEC anomalies.

Correlation coefficient / Earthquake magnitudes	Kp index	TEC (On earthquake day)		
		GPS TEC	IGS TEC	IRI TEC
3.0-3.9	-0.017	-0.067	-0.028	-0.057
4.0-4.9	-0.021	-0.086	-0.063	-0.176
5.0-higher	0.611	-0.096	-0.033	-0.271

In Table 4, the correlation coefficient among geomagnetic storms and earthquake magnitudes of 3.0-3.9, 4.0-4.9, and 5.0 or higher are -0.017, -0.021, and 0.611, respectively. In examining how geomagnetic storms relate to TEC changes on earthquake days, we divided events into the same three-magnitude groups. The correlation coefficient results for GPS TEC are -0.067, -0.086, and -0.096, respectively. For IGS TEC, they are -0.028, -0.063, and -0.033. Similarly, for IRI TEC, the results are -0.057, -0.176, and -0.271.

4. Discussions

Based on previous research and investigations into TEC anomalies and earthquake events in Thailand, we conclude that the seismo-ionosphere coupling examined occurred from 2007 to 2020. The results indicate the presence of TEC anomalies and their corresponding earthquake magnitudes. We found that earthquakes with magnitudes ranging from 3.0 to 4.9 do not exhibit a distinct correlation with TEC changes. However, for the earthquakes with a magnitude of 5.0 or higher, the moderate correlation coefficients indicate an anomaly in TEC. This location is situated on a secondary tectonic fault, resulting in fewer high-magnitude earthquake events, typically ranging in magnitude from 1.0 to 4.0 on the Richter scale. Meanwhile, there are also fewer events with a magnitude higher than 5.0. The correlation between the two factors is significant, indicating a moderate level of association. It shows that during large earthquakes, TEC values increase 3-5 days before the event, then gradually decrease to their lowest point on the day of the earthquake. Following the event, the TEC values gradually return to normal in the subsequent days. There are seven previous studies (Shah & Jin, 2015; Sharma et al., 2017; Kiyani et al., 2020; Ulukavak & Inyurt, 2020; Sharma et al., 2021a; Sharma et al., 2021b; and Nayak, 2023a) other than using earthquake events in Thailand that we compared with. These results support the research conducted by Shah and Jin (2015) on the statistical characteristics of seismo-ionospheric disturbances in GPS TEC before global earthquakes with a magnitude (Mw) equal to or greater than 5.0. The study focused on 1,492 earthquakes that occurred between 1998 and 2014. The statistical analysis of 10 days of TEC data preceding global earthquakes with Mw 5.0 or greater reveals a significant enhancement five days prior to an earthquake of Mw 6.0 or greater at a 95% confidence level. Sharma et al. (2017) conducted a study on modeling TEC anomalies as earthquake precursors using GNSS. They observed GPS data from ground-based stations, including two CORs, indicating variations in VTEC in the ionosphere a few days before seismic events. This phenomenon was evident in both low-magnitude (Mw 4.9) and higher-magnitude (Mw 7.8) earthquakes. Ulukavak and Inyurt (2020) researched seismo-ionospheric precursors of consecutive strong earthquakes in the Nepal region. The TEC values for magnitudes 2.0 to 2.5 were found to be less influenced compared to the pre-earthquake oscillations in the ionosphere. The ionospheric TEC, with magnitudes equal to or higher than 6.0, may experience a significant decline starting five days before the event. Sharma et al. (2021a) reported that the fluctuations in the TEC monitoring system were analyzed to assess their potential as earthquake precursors. Typically, TEC reactions serve as intense precursors for magnitudes exceeding 5.0. Cumulative percentages beyond Mw 5.5 indicate an increased occurrence of abnormal TEC. Seismo-ionospheric disturbances preceding Mw 6.0 earthquakes exhibit sharp increases in cumulative percentages as well, for earthquakes with a magnitude range of Mw 6.0-7.0, seismo-ionospheric disturbances associated with thrust and strike-slip events become apparent. For earthquakes with Mw > 5 specifically, the Mw 5.5 Kohima Earthquake, the Mw 6.8 Myanmar Earthquake, and the Mw 5.6 Kokrajhar Earthquake, TEC anomalies were detected 10, 12, and 13 days before the events, respectively. Analyzing all 160 earthquakes showed that the detection rate of TEC-based precursors increases with earthquake magnitude. Earthquakes of Mw < 5 were 46.50% detectable, Mw 5-6 were 81.56% detectable, and those above Mw 6 were fully detectable (Sharma et al., 2021b).

Negative correlation coefficients were observed between GPS TEC, IGS TEC, and IRI TEC and earthquakes of magnitude 5.0 or higher. The abnormality in GPS TEC, IGS TEC, and IRI TEC (-0.495, -0.501, and -0.303) indicated an association between larger earthquake events and reduced ionospheric TEC disturbance. This finding is in line with Nayak et al. (2024), who investigated ionospheric fluctuations before an Mw 7.5 earthquake on the Noto Peninsula using 30 days of IGS TEC data before the event and identified a significant TEC drop exceeding 5 TECU roughly 22-23 days before the event. A similar pattern at station MIZU further supports this geophysical connection. Positive TEC anomalies typically coincide with intense space weather, while pronounced negative anomalies emerge under calm geomagnetic conditions, reinforcing the likelihood of a seismogenic origin. Kriging interpolation confirmed that the anomalous TEC zone overlapped the epicenter. In addition, an Mw 7.1 earthquake in Nichinan revealed a comparable TEC drop, consistent with Dobrovolsky's preparation zone of 1,000-1,600 km (Dobrovolsky et al., 1979), where TEC correlation diminishes with distance. Similarly, Sharma et al. (2024) detected abnormal TEC changes within 30 days preceding the Mw 7.2 Mexico earthquake, with a notable anomaly occurring about two days prior, deviating from the 15-day average by 3-4 TECU, with the most considerable change recorded at 14.75 UTC. Moreover, data from the 200 stations showed a TEC reduction rate of 0.0017 TECU per kilometer approaching the epicenter. Spatial interpolation revealed a significantly low-TEC zone in the ionosphere above the epicenter, which aligns with dense geological fault structures, suggesting that this low-TEC area may be detectable in the earthquake preparation zone prior to the event. Nayak et al. (2023a) noted that positive and negative TEC abnormalities can appear up to a week beforehand, demonstrating a significant departure from standard ionospheric conditions. Likewise, Kiyani et al. (2020) uncovered substantial, low-intensity ionospheric anomalies within 5-10 days before and five days after the mainshock by estimating TEC from four GNSS stations during the earthquake preparation period. Moreover, Ulukavak and Inyurt (2020) observed that ionospheric anomalies can persist for up to one month, typically 15 days before and after the quake. In the five days leading up to earthquakes of Magnitude 6.0 or higher, TEC shows a notable decrease, which continues until one day before the event. According to Sharma et al. (2017), who reported significantly low TEC values 13-14 days before the first two earthquake events, there is a correlation between reduced TEC followed by subsequent high TEC and seismic activity in the Himalayan region.

In analyzing the relationship between geomagnetic storms and earthquake magnitudes, we found a positive correlation of 0.611 for events

with a magnitude of Mw 5.0 or higher, indicating that earthquakes are linked to geomagnetic activity. In contrast, no correlation was observed for minor earthquakes (M < 5.0). This result aligns with the findings of Urata et al. (2018), who investigated the connection between earthquakes and the Lorentz force, particularly around the onset of strong seismic events. They examined the Kp index, a logarithmic measure of magnetic field deviation, and employed a stacking method to align the central times of Kp surges with main earthquake shocks. Their results suggest that distinctive Kp surges often strongly correlate with earthquake onset, with the correlation varying by both region and quake magnitude. Notably, stronger earthquakes exhibit a closer association with Kp surges, reaching 100% statistical significance in the Pacific Rim, thereby emphasizing the pivotal role of geomagnetic activity in major seismic events. Furthermore, these observations are consistent with those of Duma and Vilardo (1998), who monitored seismic activity around Mount Vesuvius for approximately 25 years, recording over 7,800 events with magnitudes ranging up to 3.4. Their analysis revealed a close relationship between solar activity, the Earth's magnetic field, and local seismicity. Although they primarily presented observational evidence rather than theoretical explanations, their work supports the notion that geomagnetic variations and earthquake occurrences are interlinked, particularly in tectonically active regions. In examining the correlation between geomagnetic storms and TEC changes, specifically on earthquake days, no significant relationship was detected across TEC data derived from GPS, IGS, and IRI. This result aligns with Sharma et al. (2024), who observed Dst and Kp indices ranging from -35 to 5, suggesting that the geomagnetic storms and solar flares had a minimal impact on TEC fluctuations during their study period.

5. Conclusions

Overall, our findings suggest that ionospheric TEC anomalies can serve as a meaningful seismic precursor, particularly for earthquakes with a magnitude (Mw) of 5.0 or greater. These findings are supported by multiple studies (Sharma et al., 2017; Kiyani et al., 2020; Ulukavak & Inyurt, 2020; Nayak et al., 2023a; Sharma et al., 2024), which have consistently reported TEC fluctuations, either significant drops or surges beginning several days to weeks before mainshock occurrences. These anomalies appear most pronounced under calm geomagnetic conditions, reinforcing the likelihood that they have a seismogenic rather than solar-driven origin. Moreover, our analysis of geomagnetic storms (represented by the Kp index) reveals a strong correlation (r = 0.611) for Mw 5.0 and above, suggesting that major earthquakes can be closely tied to heightened geomagnetic activity, consistent with Urata et al. (2018). However, more minor earthquakes (Mw < 5.0) exhibit no such correlation, and day-of-event geomagnetic disturbances have a minimal effect on TEC values (Sharma et al., 2024). These collective observations, including those from local seismic networks such as Duma and Vilardo (1998) around Mount Vesuvius, highlight the broader relationship between geomagnetic variations, solar activity, and earthquake occurrences. Consequently, TEC-based monitoring augmented by geomagnetic indices emerges as a promising approach for early detection, offering actionable insights into seismic hazard preparedness. In conclusion, we applied a TEC difference analysis using data from the three TEC sources, comparing these values against an 11-day running average to detect TEC anomalies associated with geomagnetic storms (Kp). These anomalies were then evaluated to confirm whether the observed anomalies were genuinely seismo-ionospheric. Ultimately, our research guided the development of an earthquake prediction collaboration with the TMD. However, there is a need to further explore the link between seismic activity and TEC variations, either by employing other methodologies or case-by-case studies. This is particularly important given the limited number of earthquakes exceeding magnitude five within our study region, which constrains the available sample size.

6. Funding

Research Collaboration Project on Ionospheric Disturbance Southeast Asia Pacific, Department of Engineering Education, School of Industrial Education and Technology, King Mongkut's Institute of Technology Ladkrabang, Bangkok, Thailand.

7. Acknowledgements

We gratefully acknowledge the Institute of Geology and Geophysics, Chinese Academy of Sciences (IGGCAS), for providing and supporting the BG2 GNSS receivers. Appreciation is extended to the Earthquake Observation Division of the Thai Meteorological Department (TMD) for supporting the receivers and providing raw RINEX and earthquake data from Thailand. We also thank the International Reference Ionosphere (IRI) for IRI TEC data, the International GNSS Service (IGS) for TEC maps, and the Pushkov Institute of Terrestrial Magnetism, Ionosphere and Radio Wave Propagation of the Russian Academy of Sciences (IZMIRAN), the National Oceanic and Atmospheric Administration (NOAA), and the Space Weather Prediction Center (SWPC) for sharing geomagnetic storm data.

8. References

Ahmed, J., Shah, M., Awais, M., Jin, S., Ali Zafar, W., Ahmad, N., Amin, A., Ali Shah, M., & Ali, I. (2022). Seismo-ionospheric anomalies before the 2019 Mirpur earthquake from ionosonde measurements. *Advances in Space Research*, *69*(1), 26–34. https://doi.org/10.1016/j.asr.2021.07.030

Bernard, E. N., Mofield, H. O., Titov, V., Synolakis, C. E., & Gonzalez, F. I. (2006). Tsunami: Scientific frontiers, mitigation, forecasting and policy implications. Philosophical Transactions of the Royal Society A: Mathematical. *Physical and Engineering Sciences 364*(1845), 1989-2007. https://doi.org/10.1098/rsta.2006.1809.

Blewitt, G. (1990). An automatic editing algorithm for GPS data. *Geophysical Research Letters*, *17*(3), 199–202. https://doi.org/10.1029/GL017i003p00199.

Cahyadi, M. N., & Heki, K. (2013). Ionospheric disturbances of the 2007 Bengkulu and the 2005 Nias earthquakes, Sumatra, observed with a regional GPS network. *Journal of Geophysical Research: Space Physics*, *118*(4), 1777-1787. https://doi.org/10.1002/jgra.50208.

Cibeira Urtiaga, A., Berrocoso, M., Rosado, B., & Pazos, A. (2022). Detection and study of a high magnitude seismic event from GPS data: Case study of the 2011 Tohoku-Oki earthquake. *Earth Sciences Research Journal, 26*(2), 91–106. https://doi.org/10.15446/esrj.v26n2.97735.

DeSanto, J. B., Webb, S. C., Nooner, S. L., Schmidt, D. A., Crowell, B. W., Brooks, B. A., Ericksen, T. L., & Chadwell, C. D. (2023). Limited shallow slip for the 2020 Simeonof earthquake, Alaska, constrained by GNSS-Acoustic. *Geophysical Research Letters*, *50* (e2023GL105045), 1–7. https://doi.org/10.1029/2023GL105045.

Dobrovolsky, I. P., Zubkov, S. I., & Miachkin, V. I. (1979). Estimation of the size of earthquake preparation zones. *Pure and Applied Geophysics, 117*, 1025–1044. https://doi.org/10.1007/BF00876083.

Duma, G., & Vilardo, G. (1998). Seismicity cycles in the Mt. Vesuvius area and their relation to solar flux and the variations of the Earth's magnetic field. *Physics and Chemistry of the Earth, 23*(9-10), 927–931. https://doi.org/10.1016/s0079-1946(98)00121-9

Haider, S. F., Shah, M., Li, B., Jamjareegulgarn, P., de Oliveira-Júnior, J. F., & Zhou, C. (2024). Synchronized and Co-Located Ionospheric and Atmospheric Anomalies Associated with the 2023 *Mw* 7.8 Turkey Earthquake. *Remote Sensing*, *16*(2), 222. https://doi.org/10.3390/rs16020222

Heki, K. (2011). Ionospheric electron enhancement preceding the 2011 Tohoku Oki earthquake. *Geophysical Research Letters*, *38*(17), 1-5. https://doi.org/10.1029/2011GL047908

Heki, K. (2022). Ionospheric signatures of repeated passages of atmospheric waves by the 2022 Jan, 15 Hunga Tonga-Hunga Ha'apai eruption detected by QZSS-TEC observations in Japan. *Earth, Planets and Space*, *74*, 1-12. https://doi.org/10.1186/s40623-022-01674-7.

Joshi, S., Kannaujiya, S., & Joshi, U. (2023). Analysis of GNSS data for earthquake precursor studies using IONOLAB-TEC in the Himalayan region. *Quaternary*, *6*(2), 1–13. https://doi.org/10.3390/quat6020027

Kakinami, Y., Saito, H., Yamamoto, T., Chen, C.-H., Yamamoto, M.-Y., Nakajima, K., Liu, J.-Y., & Watanabe, S. (2021). Onset altitudes of co-seis-

mic ionospheric disturbances determined by multiple distributions of GNSS TEC after the foreshock of the 2011 Tohoku earthquake on March 9, 2011. *Earth and Space Science*, *8*, 1–12. https://doi.org/10.1029/2020EA001217

Kenpankho, P., Chaichana, A., Trachu, K., Supnithi, P., & Hozumi, K. (2021). Real-time GPS receiver bias estimation. *Advances in Space Research*, *68*(5), 2152–2159. https://doi.org/10.1016/j.asr.2021.01.032

Kenpankho, P., Watthanasangmechai, K., Supnithi, P., Tsugawa, T., & Maruyama, T. (2011). Comparison of GPS TEC measurements with IRI TEC prediction at the equatorial latitude station Chumphon, Thailand. *Earth Planets Space*, *63*(4), 365–370. https://doi.org/10.5047/eps.2011.01.010

Khoshgoftar, M. M., & Saradjian, M. R. (2024). Estimation of the date and magnitude of impending massive earthquakes using the integration of precursors obtainable from remote sensing data. *Earth Sciences Research Journal, 28*(4), 447–460. https://doi.org/10.15446/esrj.v28n4.105079

Kiyani, A., Shah, M., Ahmed, A., Shah, H. H., Hameed, S., Adil, M. A., & Naqvi, N. A. (2020). Seismo ionospheric anomalies possibly associated with the 2018 Mw 8.2 Fiji earthquake detected with GNSS TEC. *Journal of Geodynamics*, *140*,1–8. https://doi.org/10.1016/j.jog.2020.101782.

Li, X., Chen, C., Liang, H., Li, Y., & Zhan, W. (2023). Earthquake source parameters estimated from high-rate multi-GNSS data: a case study of the 2022 M6.9 Menyuan earthquake. *Acta Geophysica*, *71*, 625–636. https://doi.org/10.1007/s11600-022-01000-5.

Liu, J. Y., Chuo, Y. J., Shan, S. J., Tsai, Y. B., Chen, Y. I., Pulinets, S. A., & Yu, S. B. (2004). Pre-earthquake ionospheric anomalies registered by continuous GPS TEC measurements. *Annales Geophysicae*, *22*(5), 1585–1593. https://doi.org/10.5194/angeo-22-1585-2004.

Ma, G., & Maruyama, T. (2003). Derivation of TEC and estimation of instrumental biases from GEONET in Japan. *Annales Geophysicae*, *21*(10), 2083–2093. https://doi.org/10.5194/angeo-21-2083-2003.

Mukaka M. M. (2012). Statistics corner: A guide to appropriate use of correlation coefficient in medical research. *Malawi Medical Journal*, *24*(3), 69–71. PMID: 23638278; PMCID: PMC3576830.

Nachtergaele, S., Glorie, S., Morley, C., Charusiri, P., Kanjanapayont, P., Vermeesch, P., Carter, A., Van Ranst, G., & De Grave, J. (2019). Cenozoic tectonic evolution of southeastern Thailand derived from low-temperature thermochronology. *Journal of the Geological Society*, 177, 395–411. https://doi.org/10.1144/jgs2018-167.

National Oceanic and Atmospheric Administration (NOAA). (2023). NOAA forecasts quicker, stronger peaks of solar activity. https://www.weather.gov/news/102523-solar-cycle-25-update.

Nayak, K., Urias, C. L., Romero Andrade, R., Sharma, G., & Soto, M. E. T. (2023a). Analysis of Seismo-Ionospheric Irregularities Using the Available PRNs vTEC from the Closest Epicentral cGPS Stations for Large Earthquakes. *Environmental Sciences Proceedings*, *27*(1), 24. https://doi.org/10.3390/ecas2023-15144.

Nayak, K., López-Urías, C., Romero-Andrade, R., Sharma, G., Guzmán-Acevedo, G. M., Trejo-Soto, M. E. (2023b). Ionospheric Total Electron Content (TEC) anomalies as earthquake precursors: unveiling the geophysical connection leading to the 2023 Moroccan 6.8 Mw earthquake. *Geosciences*, *13*(319), 1–17. https://doi.org/10.3390/geosciences13110319.

Nayak, K., Romero-Andrade, R., Sharma, G., López-Urías, C., Trejo-Soto, M. E., & Vidal-Vega, A. I. (2024). Evaluating Ionospheric Total Electron Content (TEC) Variations as Precursors to Seismic Activity: Insights from the 2024 Noto Peninsula and Nichinan Earthquakes of Japan. *Atmosphere*, *15*(12), 1492. https://doi.org/10.3390/atmos15121492.

Nishioka, M., Saito, S., Tao, C., Shiota, D., Tsugawa, T., & Ishii, M. (2021). Statistical analysis of ionospheric total electron content (TEC): long-term estimation of extreme TEC in Japan. *Earth, Planets and Space*, *73*(1), 1–12. https://doi.org/10.1186/s40623-021-01374-8.

Ouzounov, D., Pulinets, S., Romanov, A., Tsybulya, K., Davidenko, D., Kafatos, M., & Taylor, P. (2011). Atmosphere-ionosphere response to the M9 Tohoku earthquake revealed by multi-instrument space-borne and ground observations: Preliminary results. *Earthquake Science*, *24*, 557–564. https://doi:10.1007/s11589-011-0817-z.

Palin, R. M., Searle, M. P., Morley, C. K., Charusiri, P., Horstwood, M. S. A., & Roberts, N.M.W. (2013). Timing of metamorphism of the Lansang gneiss and implications for left-lateral motion along the Mae Ping (Wang Chao) strike-slip fault, Thailand. *Journal of Asian Earth Sciences*, *76*, 120–136. https://doi.org/10.1016/j.jseaes.2013.01.021.

Peng, Z., Lei, X., Wang, D., Si, X., Mach, P., Zhong, Q., Ding, C., Deng, Y., Qin, M., & Miao, S. (2025). Mainshock rupture properties, aftershock activities and remotely triggered seismicity associated with the 2025 Mw7.7 Sagaing fault earthquake in Myanmar. *Earthquake Research Advances*, 00413. https://doi.org/10.1016/j.eqrea.2025.100413.

Pikridas, C., Bitharis, S., Katsougiannopoulos, S., Spanakaki, K., Karolos, I.-A. (2019). Study of TEC variations using permanent stations GNSS data in relation with seismic events. Application on Samothrace earthquake of 24 May 2014. *Geodesy and Cartography, 45*(3), 137–146. https://doi.org/10.3846/gac.2019.10246

Pornsopin, P., Chaila, S., Promsuk, C., Kamjudpai, C., Pananont, P., Phetkongsakul, K., Rungjaeng, W., & Boonchu, N. (2024). Seismic hazard microzonation map for the Central Plain of Thailand. *Progress in Applied Science and Technology, 14*(1), 42–53. https://doi.org/10.60101/past.2024.251551

Priyadarshi, S., Kumar, S., & Singh, A. K. (2011). Changes in total electron content associated with earthquakes (M>5) observed from GPS station, Varanasi, India. *Geomatics, Natural Hazards and Risk*, *2*(2), 123–139. https://doi.org/10.1080/19475705.2011.563390

Pulinets, S. (2004). Ionospheric precursors of earthquakes; recent advances in theory and practical applications. *Terrestrial Atmospheric and Oceanic Sciences*, *15*(3), 413–436. https://doi.org/10.3319/TAO.2004.15.3.413(EP)

Pulinets, S. A., Contreras, A. L., Bisiacchi-Giraldi, G., & Ciraolo, L. (2005). Total electron content variations in the ionosphere before the Colima, Mexico, earthquake of 21 January 2003. *Geofísica Internacional*, *44*(4), 369–377. https://orcid.org/0000-0003-3944-6686

Pushkov Institute of Terrestrial Magnetism, Ionosphere and Radio Wave Propagation Russian Academy of Sciences (IZMIRAN). (2023). Ionospheric weather, planetary storms of total electron content. https://www.izmiran.ru/ionosphere/weather/storm/

Searle, M.P., & Morley, C. K. (2011). Tectonics and thermal evolution of Thailand in the regional context of Southeast Asia. In: Ridd, M.F., Barber, A.J., Crow, M.J. (Eds.), The Geology of Thailand. The Geological Society, London, pp. 539–572. https://doi.org/10.1144/GOTH.20

Shah, M., & Jin, S. (2015). Statistical characteristics of seismo-ionospheric GPS TEC disturbances prior to global Mw ≥ 5.0 earthquakes (1998-2014). *Journal of Geodynamics*, *92*, 42–49. https://doi.org/10.1016/j.jog.2015.10.002

Shah, M., Ahmed, A., Ehsan, M., Khan, M., Tariq, M. A., Calabia, A., & Rahman, Z. U. (2020). Total electron content anomalies associated with earthquakes occurred during 1998-2019. *Acta Astronautica*, *175*, 268–276. https://doi.org/10.1016/j.actaastro.2020.06.005

Sharma, G., Champati ray, P. K., Mohanty, S., & Kannaujiya, S. (2017). Ionospheric TEC modelling for earthquakes precursors from GNSS data. *Quaternary International*, *462*, 65–74. https://doi.org/10.1016/j.quaint.2017.05.007

Sharma, G., Soubam, M., Walia, D., Nishant, N., Sarma, K. K., & Raju, P. L. N. (2021a). Development of a monitoring system for ionospheric TEC variability before the earthquakes. *Applied Computing and Geosciences*, *9*, 1–7. https://doi.org/10.1016/j.acags.2020.100052

Sharma, G., Saikia, P., Walia, D., Banerjee, P., & Raju, P.L.N. (2021b). TEC anomalies assessment for earthquakes precursors in North-Eastern India and adjoining region using GPS data acquired during 2012-2018, *Quaternary International, 575–576*, 120–129. https://doi.org/10.1016/j.quaint.2020.07.009

Sharma, G., Romero-Andrade, R., Taloor, A. K., Ganeshan, G., Sarma, K. K., & Aggarwal, S. P. (2022). 2-D ionosphere TEC anomaly before January 28, 2020, Cuba earthquake observed from a network of GPS observations data. *Arabian Journal of Geosciences, 15*(1348). https://doi.org/10.1007/s12517-022-10605-5

Sharma, G., Nayak, K., Romero-Andrade, R., Aslam, M. A. M., Sarma, K. K., & Aggarwal, S. P. (2024). Low ionosphere density above the earthquake epicentre region of Mw 7.2, El Mayor–Cucapah earthquake evident from Dense CORS Data. *Journal of the Indian Society of Remote Sensing*, *52*(3), 543–555. https://doi.org/10.1007/s12524-024-01837-x

Space Weather Prediction Center (SWPC), National Oceanic and Atmospheric Administration (NOAA). (2023). Solar cycle progression. https://www.swpc.noaa.gov/products/solar-cycle-progression

Takla, E. M. H. & Samwel, S. W. (2023). Possible connection between solar activity and local seismicity. *Terrestrial, Atmospheric and Oceanic Sciences*, *34*, 1–15. https://doi.org/10.1007/s44195-023-00042-6

Thai Meteorological Department. (2021). Focal mechanism analysis for earthquake and tsunami warnings. https://earthquake.tmd.go.th/km_view.php?id=18

Thai Meteorological Department. (2023). Development of seismic hazard microzonation map for the Central Plain of Thailand. https://earthquake.tmd.go.th/hvsr/central.php

Tiryakioglu, I., Yavasoglu, H., Ugur, M.A., Ozkaymak, C., Yilmaz, M., Kocaoglu, H., & Turgut, B. (2017). Analysis of October 23 (Mw 7.2) and November 9 (Mw 5.6), 2011 Van Earthquakes using long-term GNSS time series. *Earth Sciences Research Journal, 21*(3), 147–156. https://doi.org/10.15446/esrj.v21n3.62812

Ulukavak, M., & Inyurt, S. (2020). Seismo-ionospheric precursors of strong sequential earthquakes in Nepal region. *Acta Astronautica*, 166, 123–130. https://doi.org/10.1016/j.actaastro.2019.09.033

Urata, N., Duma, G., & Freund, F. (2018). Geomagnetic Kp index and earthquakes. *Open Journal of Earthquake Research*, *7*, 39–52. https://doi:10.4236/ojer.2018.71003.

USGS. (2008). Tectonic base map of the Sumatra subduction zone showing major faults. https://www.usgs.gov/media/images/tectonic-base-map-sumatra-subduction-zone-showing-major-faults

Watari, S. (2017). Geomagnetic storms of cycle 24 and their solar sources. *Earth Planets Space 69*(70), 1–8. https://doi.org/10.1186/s40623-017-0653-z

Xiong, X., Shan, B., Zhou, Y. M., Wei, S. J., Li, Y. D., Wang, R. J., & Zheng, Y. (2017). Coulomb stress transfer and accumulation on the Sagaing Fault, Myanmar, over the past 110 years and its implications for seismic hazard. *Geophysical Research Letters*, *44*(10), 4781–4789. https://doi.org/10.1002/2017GL072770

Xu, X., Chen, S., Zhang, S., & Dai, R. (2022). Analysis of potential precursory pattern at Earth surface and the above atmosphere and ionosphere preceding two Mw ≥ 7 earthquakes in Mexico in 2020-2021. *Earth and Space Science*, *9*(e2022EA002267), 1–24. https://doi.org/10.1029/2022EA002267